The Astrophysical Journal, 571:1015–1020, 2002 June 1

ROTATIONAL AND VIBRATIONAL EXCITATION OF CO MOLECULES BY COLLISIONS WITH ^{4}He ATOMS

Cesare Cecchi-Pestellini,[1] Enrico Bodo,[2] N. Balakrishnan,[3] and Alexander Dalgarno[4]
Harvard-Smithsonian Center for Astrophysics, 60 Garden Street, Cambridge, MA 02138
Received 2001 November 29; accepted 2002 February 4

ABSTRACT

Full close-coupled calculations are carried out of the cross sections for energy transfer between rotational levels of carbon monoxide in collision with ^{4}He atoms with energies between 5 and 600 cm^{-1}. At low energies, the cross sections are dominated by contributions from shape resonances. The calculated cross sections are in satisfactory agreement with the experimental data measured at an energy of 570 cm^{-1}. Calculations using the infinite order sudden approximation are carried out of cross sections for energy transfer between vibrational levels of CO. Vibrational energy transfer is dominated by transitions in which the vibrational quantum number changes by unity.

Subject headings: ISM: molecules — molecular data — molecular processes

1. INTRODUCTION

Rovibrational transitions of carbon monoxide are valuable diagnostic probes of diverse astrophysical environments. Rotational emission lines have been observed in diffuse, translucent, and dense interstellar clouds, in planetary nebulae, in shocked regions, and in photon dominated regions (Cernicharo 1996; Cox 1996; Nisini 1996). Vibrationally excited CO has been detected in stellar atmospheres (Uitenbroek 2000), in novae (Evans et al. 1996), in the Becklin-Neugebauer object (Scoville, Krotkov, & Wang 1980) and in supernova ejecta (Spyromilio et al. 1988; Rank et al. 1988; Meikle et al. 1993; Bouchet & Danziger 1993; Spyromilio & Leibundgut 1996; Spyromilio, Leibundgut, & Gilmozzi 2001). In these environments, collisional excitation of CO by H, He, and H_2 followed by emission is a powerful cooling mechanism (Liu & Dalgarno 1995).

Rate coefficients for collisions with H atoms based on an accurate HCO potential energy surface (Werner et al. 1995; Keller et al. 1996) have been calculated recently (Balakrishnan et al. 2001). We present here similar calculations for collisions of ^{4}He with CO on an accurate HeCO surface (Heijmen et al. 1997). Collisions of He with CO have received much attention. For astrophysical applications, the rate coefficients computed by Green & Thaddeus (1976) and McKee et al. (1982) have been employed. More reliable potential energy surfaces have become available, and the sensitivity of the cross sections to different surfaces has been explored recently (Bodo, Gianturco, & Paesani 2000). The surface of Heijmen et al. (1997) yielded rate coefficients (Reid, Simpson, & Quiney 1997; Balakrishnan, Dalgarno, & Forrey 2000) for the $\nu = 1$–0 transition that agree with the measurements of Wilson et al. (1993) performed at temperatures between 40 and 150 K to within 30%. The calculations of pure rotational excitations (Balakrishnan et al. 2000; Bodo et al. 2000) are in close agreement with the measurements of Antonova et al. (1999) carried out at center of mass energies of 72 and 89 meV.

2. CROSS SECTIONS

The CO molecule has a low rotational constant. Therefore, quantum mechanical calculations require the inclusion of many rotational functions in the basis set to obtain high accuracy in the resulting cross sections. The presence of a large number of rotational channels forced us to select the complete decoupled scheme of the IOS approximation (Kouri 1979) when treating vibrational excitation at high energies. At lower energies where vibrational excitation can be neglected and only rotational excitation within the ground vibrational manifold takes place, we were able to use the *exact* full close coupling expansion.

Rate coefficients for transitions are obtained by averaging the appropriate cross sections over a Boltzmann distribution of velocities of the incoming atom at a specified kinetic temperature T:

$$k_{v,j\rightarrow v',j'}(T) = \left(8\beta^3/\pi\mu\right)^{1/2}\int_0^\infty E_k\sigma_{v,j\rightarrow v',j'}(E_k) \times \exp(-\beta E_k)dE_k \ , \quad (1)$$

where $\beta = (k_{\rm B}T)^{-1}$, $k_{\rm B}$ is the Boltzmann constant, μ is the reduced mass of the (triatomic) colliding system, and σ is the cross section. The total energy E is related to the kinetic energy of the incoming atom according to $E = E_k + \epsilon_{vj}$, where ϵ_{vj} is the energy of the initial rovibrational level. Equation (1) simplifies when the IOS approach is used because the cross sections are not dependent upon the rotational quantum numbers. Rate coefficients for the reverse transitions may be obtained applying detailed balance:

$$k_{v',j'\rightarrow v,j}(T) = \frac{(2j+1)}{(2j'+1)}\exp[\beta(\epsilon_{v'j'} - \epsilon_{vj})]k_{v,j\rightarrow v',j'}(T) \ . \quad (2)$$

The potential energy surface adopted here is that of Heijmen et al. (1997). The IOS calculations were performed using a code that employs a Numerov algorithm to find the solution matrix in the relevant region of internuclear separation R. For these calculations, a maximum value for R of

[1] Dipartimento di Astronomia e Scienza dello Spazio, Largo E. Fermi 5, 50125 Florence, Italy; ccecchi-pestellini@cfa.harvard.edu.
[2] Department of Chemistry, University of Rome, La Sapienza, P. Aldo Moro 5, 00185 Rome, Italy; bodo@caspur.it.
[3] nbalakrishnan@cfa.harvard.edu.
[4] adalgarno@cfa.harvard.edu.

TABLE 1
CO Vibrational Energies

v	$\Delta\epsilon_v/\mathrm{cm}^{-1}$
0.....	0.0
1.....	2144.7
2.....	4263.3
3.....	6356.0
4.....	8422.6
5.....	10463.1
6.....	12477.7

approximately 20 Å together with 35 angular Gauss-Legendre quadrature points was sufficient for securing the convergence of the cross sections. The number of contributing partial waves ranges between 60 and 150 for the highest collision energies. The total number of vibrational channels included was 10. Their energy levels relative to $v = 0$ are given in Table 1. Some of the resulting cross section values for the vibrational relaxation 1–0 are compared with previous calculations in Figure 1, where we report our IOS cross sections together with the values obtained by Kobayashi et al. (2000). Our cross sections are lower that those of Kobayashi et al. (2000) by 40%–70%, the differences arising from the different surfaces adopted for the calculations. In the same figure, the rate coefficients calculated here are compared with the experimental values of Wickham-Jones, Williams, & Simpson (1987). Our coefficients are lower than the experimental values by a factor of 2.0 to 2.5. The discrepancies have been noted earlier by Reid et al. (1995, 1997) and (Kobayashi et al. 2000), who employed different potential energy surfaces. Closer agreement with the experimental

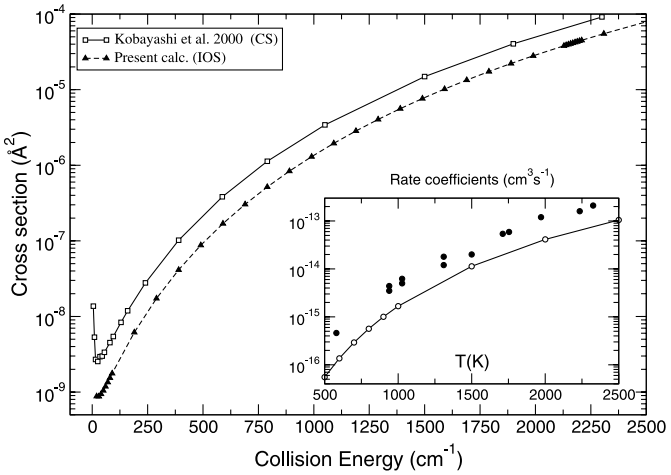

Fig. 1.—Comparison between the vibrational relaxation cross section ($1 \rightarrow 0$) calculated here and by Kobayashi et al. (2000). The inset shows a comparison between the rate coefficients calculated here *(white circles)* and experimental values from Wickham-Jones et al. (1987; *black circles*) for the same transition.

rate coefficients has been obtained recently by Krems (2001) using the same surface employed by Reid et al. (1997) and the coupled states approximation.

In Table 2, we present rate coefficients for pure vibrational quenching of the first seven vibrational levels for temperatures ranging from 500 to 5000 K. The rate coefficients for the transfer of more than one vibrational quantum are very small and vibrational energy transfer is dominated by $\Delta\nu = 1$ transitions. The rate coefficients increase rapidly with temperature initially and tend to flatten at high temperatures. The low efficiency of vibrational excitation arises

TABLE 2
Rate Coefficients for Vibrational De-Excitation $k(v \rightarrow v')$ of CO by ^{4}He Atoms (in Units of cm^3 s^{-1})

		T (K)							
v	v'	500	600	700	800	900	1000	1100	1300
1...	0	†5.5(−17)†	1.4(−16)	2.9(−16)	5.6(−16)	1.0(−15)	1.7(−15)	2.6(−15)	5.8(−15)
2...	0	1.6(−20)	6.1(−20)	1.9(−19)	5.2(−19)	1.4(−18)	3.7(−18)	1.1(−17)	8.3(−17)
3...	0	5.1(−23)	1.6(−21)	4.6(−20)	6.1(−19)	4.6(−18)	2.3(−17)	8.8(−17)	6.8(−16)
4...	0	3.9(−21)	1.9(−19)	3.1(−18)	2.5(−17)	1.3(−16)	4.6(−16)	1.3(−15)	6.6(−15)
5...	0	1.4(−18)	2.6(−17)	2.1(−16)	9.8(−16)	3.3(−15)	8.6(−15)	1.9(−14)	6.4(−14)
6...	0	4.6(−16)	3.2(−15)	1.3(−14)	3.7(−14)	8.2(−14)	1.6(−13)	2.6(−13)	5.9(−13)
2...	1	1.3(−16)	3.2(−16)	6.7(−16)	1.3(−15)	2.3(−15)	3.8(−15)	6.0(−15)	1.3(−14)
3...	1	6.6(−20)	2.5(−19)	7.7(−19)	2.0(−18)	4.9(−18)	1.1(−17)	2.1(−17)	7.0(−17)
4...	1	3.2(−22)	3.6(−21)	4.1(−20)	3.1(−19)	1.6(−18)	5.8(−18)	1.7(−17)	9.5(−17)
5...	1	1.5(−20)	2.8(−19)	2.3(−18)	1.1(−17)	3.9(−17)	1.1(−16)	2.4(−16)	9.0(−16)
6...	1	4.9(−18)	3.5(−17)	1.5(−16)	4.3(−16)	9.8(−16)	1.9(−15)	3.4(−15)	8.4(−15)
3...	2	2.3(−16)	5.6(−16)	1.2(−15)	2.3(−15)	4.1(−15)	6.7(−15)	1.1(−14)	2.3(−14)
4...	2	1.9(−19)	7.1(−19)	2.2(−18)	5.7(−18)	1.3(−17)	2.6(−17)	4.8(−17)	1.3(−16)
5...	2	1.4(−21)	9.1(−21)	4.6(−20)	1.8(−19)	5.9(−19)	1.6(−18)	3.9(−18)	1.7(−17)
6...	2	4.3(−20)	3.3(−19)	1.5(−18)	4.5(−18)	1.1(−17)	2.4(−17)	4.7(−17)	1.5(−16)
4...	3	3.7(−16)	9.0(−16)	1.9(−15)	3.6(−15)	6.4(−15)	1.0(−14)	1.6(−14)	3.3(−14)
5...	3	4.6(−19)	1.7(−18)	4.9(−18)	1.2(−17)	2.4(−17)	4.3(−17)	7.0(−17)	1.5(−16)
6...	3	3.9(−21)	1.5(−20)	4.3(−20)	1.0(−19)	2.3(−19)	5.1(−19)	1.1(−18)	6.0(−18)

TABLE 2—*Continued*

		T (K)							
v	*v′*	500	600	700	800	900	1000	1100	1300
5...	4	5.6(−16)	1.4(−15)	2.8(−15)	5.3(−15)	9.0(−15)	1.4(−14)	2.0(−14)	3.7(−14)
6...	4	9.2(−19)	2.8(−18)	6.4(−18)	1.2(−17)	2.0(−17)	2.9(−17)	4.0(−17)	6.3(−17)
6...	5	8.0(−16)	1.8(−15)	3.5(−15)	5.9(−15)	8.8(−15)	1.2(−14)	1.6(−14)	2.3(−14)
	...	1500	2000	2500	3000	3500	4000	4500	5000
1...	0	1.1(−14)	4.0(−14)	9.7(−14)	1.8(−13)	2.9(−13)	4.1(−13)	5.6(−13)	7.3(−13)
2...	0	4.5(−16)	8.0(−15)	4.8(−14)	1.6(−13)	3.9(−13)	7.7(−13)	1.3(−12)	2.0(−12)
3...	0	3.0(−15)	3.5(−14)	1.6(−13)	4.3(−13)	9.1(−13)	1.6(−12)	2.6(−12)	3.7(−12)
4...	0	2.2(−14)	1.6(−13)	5.2(−13)	1.2(−12)	2.1(−12)	3.4(−12)	4.9(−12)	6.7(−12)
5...	0	1.6(−13)	6.8(−13)	1.7(−12)	3.1(−12)	4.9(−12)	7.1(−12)	9.5(−12)	1.2(−11)
6...	0	1.1(−12)	2.9(−12)	5.3(−12)	8.2(−12)	1.1(−11)	1.5(−11)	1.8(−11)	2.2(−11)
2...	1	2.5(−14)	8.5(−14)	1.9(−13)	3.3(−13)	5.0(−13)	6.7(−13)	8.5(−13)	1.0(−12)
3...	1	1.9(−16)	1.3(−15)	5.7(−15)	1.8(−14)	4.4(−14)	9.2(−14)	1.7(−13)	2.7(−13)
4...	1	3.4(−16)	3.2(−15)	1.4(−14)	4.1(−14)	9.5(−14)	1.8(−13)	3.1(−13)	4.8(−13)
5...	1	2.4(−15)	1.4(−14)	4.5(−14)	1.1(−13)	2.2(−13)	3.8(−13)	5.9(−13)	8.6(−13)
6...	1	1.7(−14)	5.9(−14)	1.4(−13)	2.9(−13)	5.0(−13)	7.9(−13)	1.1(−12)	1.5(−12)
3...	2	4.2(−14)	1.3(−13)	2.5(−13)	4.0(−13)	5.5(−13)	6.8(−13)	8.0(−13)	9.1(−13)
4...	2	2.7(−16)	9.8(−16)	2.8(−15)	7.3(−15)	1.7(−14)	3.6(−14)	6.5(−14)	1.1(−13)
5...	2	5.8(−17)	6.7(−16)	3.8(−15)	1.3(−14)	3.3(−14)	6.7(−14)	1.2(−13)	1.8(−13)
6...	2	3.9(−16)	2.8(−15)	1.2(−14)	3.5(−14)	7.6(−14)	1.4(−13)	2.2(−13)	3.3(−13)
4...	3	5.7(−14)	1.5(−13)	2.5(−13)	3.5(−13)	4.4(−13)	5.2(−13)	5.8(−13)	6.4(−13)
5...	3	2.5(−16)	6.9(−16)	2.0(−15)	6.0(−15)	1.6(−14)	3.4(−14)	6.3(−14)	1.0(−13)
6...	3	2.8(−17)	5.3(−16)	3.5(−15)	1.3(−14)	3.3(−14)	6.7(−14)	1.2(−13)	1.8(−13)
5...	4	5.8(−14)	1.1(−13)	1.7(−13)	2.0(−13)	2.3(−13)	2.5(−13)	2.7(−13)	2.8(−13)
6...	4	8.9(−17)	2.3(−16)	9.5(−16)	3.4(−15)	8.8(−15)	1.8(−14)	3.3(−14)	5.2(−14)
6...	5	3.1(−14)	4.5(−14)	5.2(−14)	5.6(−14)	5.7(−14)	5.7(−14)	5.8(−14)	5.8(−14)
	...	...	...	...	...	...	...	...	...

† Numbers in parentheses are powers of 10.

TABLE 3
CO Rotational Energies

J	$\Delta\epsilon_{vJ}/\mathrm{cm}^{-1}$
1.....	3.85
2.....	11.54
3.....	23.07
4.....	38.45
5.....	57.68
6.....	80.75
7.....	107.66
8.....	138.42
9.....	173.03
10.....	211.48
11.....	253.77
12.....	299.91
13.....	349.90
14.....	403.73

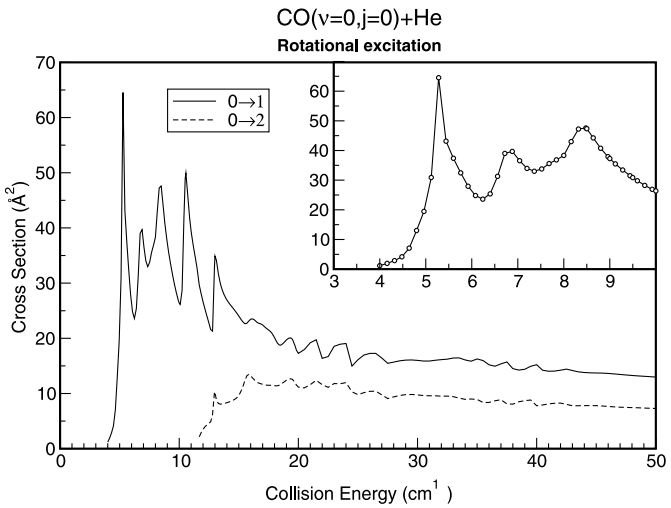

Fig. 2.—Rotational excitation cross section as a function of collision energy. The $0 \rightarrow 1$ and $0 \rightarrow 2$ transitions are displayed. *Upper right inset*: resonance structure of the $0 \rightarrow 1$ transition is shown on an enhanced energy scale.

TABLE 4

RATE COEFFICIENTS FOR ROTATIONAL DE-EXCITATION $k(J \rightarrow J')$ OF CO BY ^{4}He ATOMS (IN UNITS OF cm^3 s^{-1})

		T (K)									
J	J'	5	10	20	40	60	80	100	200	300	500
1.....	0	†3.4(−11)†	3.2(−11)	3.0(−11)	2.8(−11)	2.7(−11)	2.6(−11)	2.6(−11)	2.5(−11)	2.5(−11)	2.6(−11)
2.....	0	1.3(−11)	1.3(−11)	1.2(−11)	1.1(−11)	1.1(−11)	1.1(−11)	1.1(−11)	1.4(−11)	1.6(−11)	1.9(−11)
3.....	0	6.2(−12)	6.6(−12)	7.2(−12)	8.5(−12)	9.5(−12)	1.0(−11)	1.1(−11)	1.2(−11)	1.3(−11)	1.4(−11)
4.....	0	1.8(−12)	1.9(−12)	1.9(−12)	2.0(−12)	2.1(−12)	2.1(−12)	2.2(−12)	2.6(−12)	3.1(−12)	4.0(−12)
5.....	0	1.4(−12)	1.5(−12)	1.8(−12)	2.4(−12)	2.9(−12)	3.3(−12)	3.7(−12)	4.9(−12)	5.6(−12)	6.8(−12)
6.....	0	5.8(−13)	5.6(−13)	6.0(−13)	7.6(−13)	9.3(−13)	1.1(−12)	1.2(−12)	1.5(−12)	1.7(−12)	1.9(−12)
7.....	0	3.4(−13)	3.8(−13)	4.6(−13)	6.6(−13)	8.9(−13)	1.1(−12)	1.3(−12)	1.9(−12)	2.3(−12)	2.8(−12)
8.....	0	1.3(−13)	1.4(−13)	1.7(−13)	2.6(−13)	3.9(−13)	5.1(−13)	6.4(−13)	1.1(−12)	1.4(−12)	1.7(−12)
9.....	0	6.5(−14)	7.4(−14)	9.5(−14)	1.6(−13)	2.4(−13)	3.2(−13)	4.1(−13)	7.6(−13)	9.8(−13)	1.3(−12)
10...	0	3.4(−14)	3.6(−14)	4.5(−14)	8.0(−14)	1.3(−13)	2.0(−13)	2.7(−13)	6.2(−13)	8.8(−13)	1.2(−12)
11...	0	1.4(−14)	1.5(−14)	2.0(−14)	3.7(−14)	6.4(−14)	9.7(−14)	1.3(−13)	3.1(−13)	4.4(−13)	5.9(−13)
12...	0	6.7(−15)	8.1(−15)	1.1(−14)	2.2(−14)	4.1(−14)	6.7(−14)	9.7(−14)	2.4(−13)	3.3(−13)	4.4(−13)
13...	0	2.8(−15)	3.4(−15)	4.9(−15)	9.4(−15)	1.7(−14)	2.6(−14)	3.6(−14)	7.6(−14)	1.0(−13)	1.3(−13)
14...	0	2.1(−15)	2.2(−15)	3.0(−15)	6.3(−15)	1.2(−14)	1.8(−14)	2.4(−14)	4.5(−14)	5.5(−14)	6.5(−14)
2.....	1	4.2(−11)	4.5(−11)	4.5(−11)	4.6(−11)	4.7(−11)	4.8(−11)	4.9(−11)	5.0(−11)	5.2(−11)	5.7(−11)
3.....	1	2.3(−11)	2.2(−11)	2.0(−11)	1.8(−11)	1.8(−11)	1.8(−11)	1.9(−11)	2.2(−11)	2.6(−11)	3.2(−11)
4.....	1	1.3(−11)	1.4(−11)	1.5(−11)	1.7(−11)	1.8(−11)	2.0(−11)	2.1(−11)	2.4(−11)	2.7(−11)	3.1(−11)
5.....	1	3.4(−12)	3.6(−12)	3.7(−12)	4.1(−12)	4.4(−12)	4.6(−12)	4.9(−12)	6.0(−12)	7.0(−12)	8.5(−12)
6.....	1	4.2(−12)	3.9(−12)	4.1(−12)	5.0(−12)	5.9(−12)	6.8(−12)	7.5(−12)	1.0(−11)	1.2(−11)	1.4(−11)
7.....	1	1.0(−12)	1.1(−12)	1.2(−12)	1.6(−12)	2.0(−12)	2.4(−12)	2.7(−12)	3.9(−12)	4.6(−12)	5.5(−12)
8.....	1	7.8(−13)	8.3(−13)	9.7(−13)	1.4(−12)	1.8(−12)	2.2(−12)	2.6(−12)	4.0(−12)	4.8(−12)	5.9(−12)
9.....	1	3.0(−13)	3.2(−13)	3.8(−13)	5.7(−13)	8.3(−13)	1.1(−12)	1.4(−12)	2.6(−12)	3.4(−12)	4.5(−12)
10...	1	1.8(−13)	1.8(−13)	2.2(−13)	3.4(−13)	5.0(−13)	6.7(−13)	8.5(−13)	1.6(−12)	2.1(−12)	2.7(−12)
11...	1	8.3(−14)	8.8(−14)	1.1(−13)	1.8(−13)	2.9(−13)	4.3(−13)	5.8(−13)	1.3(−12)	1.8(−12)	2.5(−12)
12...	1	3.0(−14)	3.6(−14)	4.9(−14)	8.6(−14)	1.4(−13)	2.1(−13)	2.9(−13)	6.5(−13)	8.8(−13)	1.1(−12)
13...	1	1.8(−14)	2.1(−14)	2.8(−14)	4.9(−14)	8.3(−14)	1.2(−13)	1.7(−13)	3.4(−13)	4.5(−13)	5.6(−13)
14...	1	7.8(−15)	8.3(−15)	1.1(−14)	2.2(−14)	3.9(−14)	5.9(−14)	7.9(−14)	1.4(−13)	1.8(−13)	2.1(−13)
3.....	2	4.6(−11)	4.9(−11)	5.0(−11)	5.1(−11)	5.2(−11)	5.3(−11)	5.4(−11)	5.8(−11)	6.1(−11)	6.8(−11)
4.....	2	2.7(−11)	2.7(−11)	2.4(−11)	2.2(−11)	2.2(−11)	2.2(−11)	2.3(−11)	2.7(−11)	3.1(−11)	3.7(−11)
5.....	2	1.7(−11)	1.8(−11)	1.9(−11)	2.1(−11)	2.3(−11)	2.4(−11)	2.6(−11)	3.0(−11)	3.3(−11)	3.7(−11)
6.....	2	6.3(−12)	5.7(−12)	5.4(−12)	5.3(−12)	5.6(−12)	5.9(−12)	6.3(−12)	8.2(−12)	9.8(−12)	1.2(−11)
7.....	2	4.7(−12)	5.0(−12)	5.5(−12)	6.6(−12)	7.7(−12)	8.6(−12)	9.5(−12)	1.2(−11)	1.5(−11)	1.7(−11)
8.....	2	1.6(−12)	1.7(−12)	1.8(−12)	2.2(−12)	2.6(−12)	3.1(−12)	3.5(−12)	5.3(−12)	6.4(−12)	8.0(−12)
9.....	2	1.1(−12)	1.2(−12)	1.4(−12)	1.9(−12)	2.4(−12)	2.9(−12)	3.3(−12)	5.0(−12)	6.1(−12)	7.5(−12)
10...	2	5.7(−13)	5.6(−13)	6.2(−13)	8.5(−13)	1.2(−12)	1.5(−12)	1.8(−12)	3.3(−12)	4.4(−12)	5.6(−12)
11...	2	2.7(−13)	2.9(−13)	3.4(−13)	5.0(−13)	7.0(−13)	9.2(−13)	1.1(−12)	2.0(−12)	2.6(−12)	3.4(−12)
12...	2	1.2(−13)	1.4(−13)	1.8(−13)	2.8(−13)	4.3(−13)	6.1(−13)	8.1(−13)	1.7(−12)	2.2(−12)	2.8(−12)
13...	2	5.2(−14)	6.1(−14)	7.9(−14)	1.3(−13)	1.9(−13)	2.6(−13)	3.4(−13)	6.1(−13)	7.7(−13)	9.4(−13)
14...	2	3.5(−14)	3.6(−14)	4.4(−14)	7.9(−14)	1.3(−13)	1.9(−13)	2.5(−13)	4.3(−13)	5.2(−13)	6.1(−13)
4.....	3	5.3(−11)	5.4(−11)	5.4(−11)	5.4(−11)	5.4(−11)	5.5(−11)	5.6(−11)	6.0(−11)	6.4(−11)	7.1(−11)
5.....	3	2.4(−11)	2.5(−11)	2.5(−11)	2.3(−11)	2.3(−11)	2.3(−11)	2.4(−11)	2.9(−11)	3.4(−11)	4.1(−11)
6.....	3	3.3(−11)	2.8(−11)	2.6(−11)	2.6(−11)	2.7(−11)	2.8(−11)	2.9(−11)	3.3(−11)	3.6(−11)	4.1(−11)
7.....	3	5.5(−12)	5.8(−12)	5.9(−12)	6.0(−12)	6.3(−12)	6.6(−12)	7.0(−12)	9.4(−12)	1.1(−11)	1.5(−11)
8.....	3	6.3(−12)	6.5(−12)	7.0(−12)	8.1(−12)	9.2(−12)	1.0(−11)	1.1(−11)	1.4(−11)	1.6(−11)	1.9(−11)
9.....	3	2.0(−12)	2.1(−12)	2.3(−12)	2.7(−12)	3.2(−12)	3.7(−12)	4.1(−12)	6.0(−12)	7.3(−12)	9.0(−12)
10...	3	1.8(−12)	1.8(−12)	1.9(−12)	2.4(−12)	2.9(−12)	3.5(−12)	3.9(−12)	5.7(−12)	6.8(−12)	8.2(−12)
11...	3	7.3(−13)	7.5(−13)	8.4(−13)	1.1(−12)	1.5(−12)	1.9(−12)	2.2(−12)	3.8(−12)	4.9(−12)	6.1(−12)
12...	3	3.2(−13)	3.7(−13)	4.5(−13)	6.6(−13)	9.1(−13)	1.2(−12)	1.5(−12)	2.5(−12)	3.2(−12)	3.9(−12)
13...	3	1.7(−13)	1.9(−13)	2.4(−13)	3.6(−13)	5.0(−13)	6.7(−13)	8.3(−13)	1.4(−12)	1.8(−12)	2.2(−12)
14...	3	7.9(−14)	8.0(−14)	9.7(−14)	1.6(−13)	2.6(−13)	3.6(−13)	4.5(−13)	7.6(−13)	9.2(−13)	1.1(−12)
5.....	4	5.1(−11)	5.4(−11)	5.5(−11)	5.6(−11)	5.6(−11)	5.7(−11)	5.8(−11)	6.1(−11)	6.5(−11)	7.3(−11)
6.....	4	3.8(−11)	3.2(−11)	2.8(−11)	2.5(−11)	2.4(−11)	2.4(−11)	2.5(−11)	3.1(−11)	3.6(−11)	4.4(−11)
7.....	4	2.5(−11)	2.6(−11)	2.7(−11)	2.8(−11)	2.9(−11)	3.0(−11)	3.1(−11)	3.5(−11)	3.8(−11)	4.3(−11)
8.....	4	6.5(−12)	6.7(−12)	6.8(−12)	6.8(−12)	6.9(−12)	7.2(−12)	7.6(−12)	9.9(−12)	1.2(−11)	1.5(−11)
9.....	4	7.0(−12)	7.4(−12)	8.1(−12)	9.2(−12)	1.0(−11)	1.1(−11)	1.2(−11)	1.5(−11)	1.7(−11)	2.0(−11)
10...	4	3.0(−12)	2.9(−12)	2.9(−12)	3.3(−12)	3.8(−12)	4.2(−12)	4.7(−12)	6.4(−12)	7.6(−12)	9.2(−12)
11...	4	1.9(−12)	2.0(−12)	2.2(−12)	2.8(−12)	3.4(−12)	3.9(−12)	4.4(−12)	6.1(−12)	7.2(−12)	8.4(−12)

TABLE 4—*Continued*

		T (K)									
J	*J′*	5	10	20	40	60	80	100	200	300	500
12...	4	7.7(−13)	8.7(−13)	1.0(−12)	1.4(−12)	1.8(−12)	2.3(−12)	2.7(−12)	4.5(−12)	5.5(−12)	6.8(−12)
13...	4	3.9(−13)	4.4(−13)	5.4(−13)	7.5(−13)	9.8(−13)	1.2(−12)	1.4(−12)	2.1(−12)	2.5(−12)	3.0(−12)
14...	4	2.4(−13)	2.4(−13)	2.9(−13)	4.5(−13)	6.7(−13)	9.1(−13)	1.1(−12)	1.8(−12)	2.2(−12)	2.5(−12)
6.....	5	6.6(−11)	6.7(−11)	6.4(−11)	6.1(−11)	6.0(−11)	6.0(−11)	6.1(−11)	6.3(−11)	6.7(−11)	7.4(−11)
7.....	5	2.2(−11)	2.4(−11)	2.4(−11)	2.3(−11)	2.3(−11)	2.4(−11)	2.5(−11)	3.1(−11)	3.6(−11)	4.5(−11)
8.....	5	2.8(−11)	2.9(−11)	2.9(−11)	3.0(−11)	3.1(−11)	3.2(−11)	3.3(−11)	3.6(−11)	3.9(−11)	4.4(−11)
9.....	5	6.7(−12)	7.0(−12)	7.2(−12)	7.3(−12)	7.4(−12)	7.7(−12)	8.0(−12)	1.0(−11)	1.2(−11)	1.5(−11)
10...	5	9.6(−12)	9.0(−12)	9.2(−12)	1.0(−11)	1.1(−11)	1.2(−11)	1.3(−11)	1.6(−11)	1.8(−11)	2.1(−11)
11...	5	3.1(−12)	3.1(−12)	3.3(−12)	3.8(−12)	4.3(−12)	4.8(−12)	5.2(−12)	7.0(−12)	8.1(−12)	9.6(−12)
12...	5	1.8(−12)	2.0(−12)	2.4(−12)	3.1(−12)	3.8(−12)	4.5(−12)	5.1(−12)	7.3(−12)	8.6(−12)	1.0(−11)
13...	5	8.6(−13)	9.7(−13)	1.2(−12)	1.5(−12)	1.9(−12)	2.2(−12)	2.6(−12)	3.7(−12)	4.4(−12)	5.1(−12)
14...	5	4.6(−13)	4.6(−13)	5.3(−13)	7.8(−13)	1.1(−12)	1.4(−12)	1.7(−12)	2.6(−12)	3.1(−12)	3.5(−12)
7.....	6	6.5(−11)	6.7(−11)	6.6(−11)	6.4(−11)	6.3(−11)	6.3(−11)	6.3(−11)	6.5(−11)	6.8(−11)	7.6(−11)
8.....	6	2.1(−11)	2.3(−11)	2.3(−11)	2.3(−11)	2.3(−11)	2.4(−11)	2.5(−11)	3.1(−11)	3.6(−11)	4.5(−11)
9.....	6	2.7(−11)	2.9(−11)	3.0(−11)	3.1(−11)	3.3(−11)	3.4(−11)	3.4(−11)	3.8(−11)	4.1(−11)	4.6(−11)
10...	6	9.2(−12)	8.4(−12)	8.1(−12)	8.0(−12)	8.0(−12)	8.3(−12)	8.6(−12)	1.1(−11)	1.3(−11)	1.6(−11)
11...	6	8.5(−12)	8.6(−12)	9.3(−12)	1.1(−11)	1.2(−11)	1.3(−11)	1.4(−11)	1.6(−11)	1.8(−11)	2.1(−11)
12...	6	2.8(−12)	3.1(−12)	3.5(−12)	4.2(−12)	4.9(−12)	5.5(−12)	6.0(−12)	8.0(−12)	9.1(−12)	1.1(−11)
13...	6	1.8(−12)	2.0(−12)	2.4(−12)	3.1(−12)	3.6(−12)	4.1(−12)	4.5(−12)	5.8(−12)	6.5(−12)	7.4(−12)
14...	6	1.1(−12)	1.1(−12)	1.2(−12)	1.7(−12)	2.4(−12)	3.0(−12)	3.6(−12)	5.4(−12)	6.4(−12)	7.3(−12)
8.....	7	7.1(−11)	7.2(−11)	7.0(−11)	6.8(−11)	6.6(−11)	6.6(−11)	6.6(−11)	6.7(−11)	7.0(−11)	7.7(−11)
9.....	7	1.9(−11)	2.0(−11)	2.1(−11)	2.1(−11)	2.2(−11)	2.3(−11)	2.4(−11)	3.0(−11)	3.6(−11)	4.4(−11)
10...	7	3.6(−11)	3.3(−11)	3.2(−11)	3.3(−11)	3.4(−11)	3.5(−11)	3.5(−11)	3.9(−11)	4.2(−11)	4.7(−11)
11...	7	8.0(−12)	8.0(−12)	8.1(−12)	8.3(−12)	8.5(−12)	8.7(−12)	9.1(−12)	1.1(−11)	1.3(−11)	1.5(−11)
12...	7	6.9(−12)	7.8(−12)	9.0(−12)	1.1(−11)	1.2(−11)	1.4(−11)	1.5(−11)	1.9(−11)	2.1(−11)	2.5(−11)
13...	7	2.8(−12)	3.2(−12)	3.6(−12)	4.2(−12)	4.7(−12)	5.2(−12)	5.5(−12)	6.8(−12)	7.5(−12)	8.4(−12)
14...	7	1.9(−12)	1.8(−12)	2.1(−12)	2.8(−12)	3.6(−12)	4.3(−12)	4.9(−12)	7.0(−12)	8.0(−12)	9.0(−12)
9.....	8	7.0(−11)	7.3(−11)	7.2(−11)	7.0(−11)	6.9(−11)	6.8(−11)	6.8(−11)	6.9(−11)	7.2(−11)	8.0(−11)
10...	8	2.5(−11)	2.2(−11)	2.1(−11)	2.1(−11)	2.1(−11)	2.2(−11)	2.4(−11)	3.1(−11)	3.8(−11)	4.7(−11)
11...	8	2.9(−11)	2.9(−11)	3.0(−11)	3.2(−11)	3.4(−11)	3.5(−11)	3.6(−11)	3.9(−11)	4.2(−11)	4.7(−11)
12...	8	6.7(−12)	7.4(−12)	8.1(−12)	8.7(−12)	9.0(−12)	9.3(−12)	9.6(−12)	1.1(−11)	1.2(−11)	1.3(−11)
13...	8	6.2(−12)	7.1(−12)	8.2(−12)	9.8(−12)	1.1(−11)	1.2(−11)	1.3(−11)	1.5(−11)	1.6(−11)	1.8(−11)
14...	8	3.5(−12)	3.4(−12)	3.8(−12)	5.0(−12)	6.4(−12)	7.7(−12)	8.8(−12)	1.2(−11)	1.4(−11)	1.6(−11)
10...	9	1.1(−10)	9.2(−11)	8.2(−11)	7.5(−11)	7.3(−11)	7.2(−11)	7.2(−11)	7.2(−11)	7.4(−11)	8.2(−11)
11...	9	1.8(−11)	1.9(−11)	1.9(−11)	2.0(−11)	2.0(−11)	2.1(−11)	2.3(−11)	3.0(−11)	3.6(−11)	4.5(−11)
12...	9	2.2(−11)	2.5(−11)	2.8(−11)	3.1(−11)	3.4(−11)	3.6(−11)	3.7(−11)	4.4(−11)	4.8(−11)	5.6(−11)
13...	9	6.6(−12)	7.3(−12)	8.0(−12)	8.5(−12)	8.7(−12)	8.9(−12)	9.1(−12)	1.0(−11)	1.1(−11)	1.2(−11)
14...	9	6.4(−12)	6.3(−12)	6.8(−12)	8.6(−12)	1.0(−11)	1.2(−11)	1.3(−11)	1.7(−11)	1.9(−11)	2.2(−11)
11...	10	8.0(−11)	7.9(−11)	7.7(−11)	7.5(−11)	7.4(−11)	7.4(−11)	7.3(−11)	7.5(−11)	7.8(−11)	8.7(−11)
12...	10	1.4(−11)	1.6(−11)	1.7(−11)	1.8(−11)	1.9(−11)	2.0(−11)	2.1(−11)	2.7(−11)	3.1(−11)	3.8(−11)
13...	10	1.9(−11)	2.2(−11)	2.5(−11)	2.8(−11)	3.0(−11)	3.1(−11)	3.2(−11)	3.6(−11)	3.8(−11)	4.2(−11)
14...	10	8.5(−12)	8.3(−12)	9.0(−12)	1.1(−11)	1.3(−11)	1.5(−11)	1.7(−11)	2.3(−11)	2.6(−11)	3.0(−11)
12...	11	6.3(−11)	7.0(−11)	7.4(−11)	7.6(−11)	7.6(−11)	7.6(−11)	7.6(−11)	7.9(−11)	8.4(−11)	9.5(−11)
13...	11	1.4(−11)	1.6(−11)	1.7(−11)	1.8(−11)	1.8(−11)	1.9(−11)	2.1(−11)	2.6(−11)	3.1(−11)	3.8(−11)
14...	11	2.2(−11)	2.2(−11)	2.3(−11)	2.7(−11)	3.1(−11)	3.4(−11)	3.7(−11)	4.5(−11)	5.0(−11)	5.8(−11)
13...	12	6.2(−11)	6.9(−11)	7.3(−11)	7.5(−11)	7.5(−11)	7.4(−11)	7.4(−11)	7.7(−11)	8.1(−11)	9.2(−11)
14...	12	1.9(−11)	1.8(−11)	1.9(−11)	2.2(−11)	2.4(−11)	2.7(−11)	2.9(−11)	3.8(−11)	4.3(−11)	5.1(−11)
14...	13	9.2(−11)	8.8(−11)	8.9(−11)	9.6(−11)	1.0(−10)	1.1(−10)	1.1(−10)	1.3(−10)	1.5(−10)	1.7(−10)

† Numbers in parentheses are powers of 10.

because of the small distortion induced by the approach of the He atom of the large bond constant of CO.

Close coupling calculations of rotational excitation cross sections were performed using a scattering code was written by one of us (E. B.). The code uses the propagator subroutines contained in the MOLSCAT code (Hutson & Green 1994) and it has been written with the use of MPI libraries and can achieve some degree of parallelization. The code was employed on a four-processor Compaq Digital Alpha machine. The hybrid log-derivative propagator of Alexander & Manolopoulos (1987) with a variable step size was used for energies between 5 and 600 cm^{-1}. The number of partial waves ranged between 25 and 60 in order to obtain convergence over the entire energy range. The number of rotational channels was 24, ensuring that at least seven closed channels were included in the basis set at the higher energies. The energies of the first 15 levels relative to $j = 0$ are presented in Table 3.

Cross sections for the two lowest rotational transitions from the ground rovibrational state of CO are shown in Figure 2 as functions of the collision energy. The cross sections reflect the presence of a large number of shape resonances close to the threshold, which influence the collisional rates at low temperature (Reid et al. 1997; Balakrishnan et al. 2000). These resonances are apparent in the calculations of Green & Thaddeus (1976).

In Table 4, we present rate coefficients for pure rotational excitation for the first 15 rotational levels in the temperature range 5 to 500 K. They agree to within 30% with those of Green & Thaddeus (1976). The rate coefficients are large because the potential energy surface is highly anisotropic, although they are smaller than those from collisions with atomic hydrogen (Green & Thaddeus 1976; Balakrishnan et al. 2001) for which the interaction potential has a deep well. They are comparable to those from collisions with ortho and para hydrogen (Flower 2001; Mengel, De Lucia, & Herbst 2001), some being larger and some being smaller.

This research has been supported by the Division of Astronomy of the US National Science Foundation. E. B. thanks the National Institute for the Physics of Matter (INFM) and the Ministry for University and Research (MURST) for partially funding his stay at the CfA while this work was carried out.

REFERENCES

Alexander, M. H., & Manolopoulos, D. E. 1987, J. Chem. Phys., 86, 2044
Antonova, S., Lin, A., Tsakotellis, A. P., & McBane, G. C. 1999, J. Chem. Phys., 110, 2384
Balakrishnan, N., Dalgarno, A., & Forrey, R. C. 2000, J. Chem. Phys., 113, 621
Balakrishnan, N., Yan, M., & Dalgarno, A. 2001, ApJ, 568, 443
Bodo, E., Gianturco, F. A., & Paesani, F. 2000, J. Phys. Chem., 214, 1013
Bouchet, P., & Danziger, I. J. 1993, A&A, 273, 451
Cernicharo, J. 1996, A&A, 315, L201
Cox, P. 1996, A&A, 315, L256
Evans, A., Geballe, T. R., Rawlings, J. M. C., & Scott, A. D. 1996, MNRAS, 282, 1049
Flower, D. R. 2001, J. Phys. B, 34, 2731
Green, S., & Thaddeus, P. 1976, ApJ, 205, 766
Heijmen, T. G., Moszynski, R., Wormer, P., & van der Avoird, A. 1997, J. Chem. Phys., 107, 9921
Hutson, J. M., & Green, S. 1994, MOLSCAT Computer Code Version 14 (distributed by Collaborative Computational Project No. 6 of the Engineering and Physical Sciences Research Council, UK)
Keller, H. M., Werner, H. J., Bauer, C., & Rosmus, P. 1996, J. Chem. Phys., 105, 4983
Kobayashi, K., Amos, R. D., Reid, J. P., Quiney, H. M., & Simpson, C. J. S. M. 2000, Mol. Phys., 98, 1995
Kouri, D. J. 1979, in Atom Molecule Collision Theory, ed. R. B. Bernstein (New York: Plenum Press), 301
Krems, R. V. 2001, J. Chem. Phys., 116, 4517
Liu, W., & Dalgarno, A. 1995, ApJ, 454, 472
McKee, C. F., Storey, J. W., Watson, D. M., & Green, S. 1982, ApJ, 259, 647
Meikle, W. P. S., Spyromilio, J., Allen, D. A., Varani, G. F., & Cumming, R. J. 1993, MNRAS, 261, 535
Mengel, M., De Lucia, F. C., & Herbst, E. 2001, Canadian J. Phys., 79, 579
Nisini, B. 1996, A&A, 315, L321
Rank, D. M., Pinto, P. A., Woosley, S. E., Bergman, J. D., Witteborn, F. C., & Axelrod, T. S. 1988, Nature, 331, 505
Reid, J. P., Simpson, C. J. M., & Quiney, H. M. 1997, J. Chem. Phys., 107, 9929
Reid, J. P., Simpson, C. J. M., Quiney, H. M., & Hutson, J. M. 1995, J. Chem. Phys., 103, 2528
Scoville, N. Z., Krotkov, R., & Wang, D. 1980, ApJ, 240, 929
Spyromilio, J., & Leibundgut, B. 1996, MNRAS, 283, 89
Spyromilio, J., Leibundgut, B., & Gilmozzi, R. 2001, A&A, 376, 188
Spyromilio, J., Meikle, W. P. S., Lerner, R. C. M., & Allen, D. A. 1988, Nature, 334, 327
Uitenbroek, H. 2000, ApJ, 536, 481
Werner, H. J., Bauer, C., Rosmus, P., Keller, H. M., Stumpf, M., & Schinke, R. 1995, J. Chem. Phys., 102, 3593
Wickham-Jones, C. T., Williams, H. T., & Simpson, C. J. S. M. 1987, J. Chem. Phys., 87, 5294
Wilson, G. J., Turnidge, M. L., Solodukhin, A. S., & Simpson, C. J. S. M. 1993, Chem. Phys. Lett., 207, 521